Journal of Nuclear Medicine, published on June 11, 2015 as doi:10.2967/jnumed.115.154336

Title: ^{18}F-DCFBC PET/CT for PSMA-based Detection and Characterization of Primary Prostate Cancer

Running Foot: ^{18}F-DCFBC Imaging of Primary Prostate Cancer

Authors: Steven P. Rowe[1*], Kenneth L. Gage[1*], Sheila F. Faraj[2], Katarzyna J. Macura[1,3,4], Toby C. Cornish[2], Nilda Gonzalez-Roibon[2], Gunes Guner[2], Enrico Munari[2], Alan W. Partin[3], Christian P. Pavlovich[3], Misop Han[3], H. Ballentine Carter[3], Trinity J. Bivalacqua[3], Amanda Blackford[1], Daniel Holt[1], Robert F. Dannals[1], George J. Netto[2,3,4], Martin A. Lodge[1], Ronnie C. Mease[1], Martin G. Pomper[1], and Steve Y. Cho[1,4,5]

[1]The Russell H. Morgan Department of Radiology and Radiological Science, [2]Department of Pathology, and [3]The James Buchanan Brady Urological Institute and Department of Urology, and [4]Sidney Kimmel Comprehensive Cancer Center, Johns Hopkins Medical Institutions, Baltimore, MD, USA. [5]Present address: Department of Radiology, University of Wisconsin School of Medicine and Public Health, Madison, WI, USA.

*Both authors contributed equally to this work

Funding: Prostate Cancer Foundation, Movember Creativity Award, Brady Patana Research Fund, EB006351, and CA134675.

Disclosures:

First Author:
Steven P. Rowe, M.D., Ph.D.
Resident
The Russell H. Morgan Department of Radiology and Radiological Science, The Johns Hopkins Hospital
601 N. Caroline St., Room 3150, Baltimore, MD 21287
(p) (410) 955-6500; srowe8@jhmi.edu

Corresponding Author:
Steve Y. Cho, M.D.
1111 Highland Avenue, WIMR 7139
Madison, WI 53705
Office: (608) 263-5048
Fax: (608) 265-7390
Email: scho@uwhealth.org

Word Count:
(Limit 5000, including figures and tables and legends)

ABSTRACT

We previously demonstrated the ability to detect metastatic prostate cancer using ^{18}F-DCFBC (DCFBC), a low-molecular-weight radiotracer that targets the prostate-specific membrane antigen (PSMA). PSMA has been shown to be associated with higher Gleason grade and more aggressive disease. An imaging biomarker able to detect clinically significant high-grade primary prostate cancer reliably would address an unmet clinical need by allowing for risk-adapted patient management.

Methods: We enrolled 13 patients with primary prostate cancer who were imaged with DCFBC PET prior to scheduled prostatectomy, with 12 of these patients also undergoing pelvic prostate MRI. Prostate DCFBC PET was correlated with MRI and histological and immunohistochemical (IHC) analysis on a prostate segment (12 regions) and dominant lesion basis. There were no incidental extraprostatic findings on PET suspicious for metastatic disease.

Results: MRI was more sensitive than DCFBC PET for detection of primary prostate cancer on a per-segment (sensitivities of up to 0.17 and 0.39 for PET and MRI, respectively) and per-dominant lesion analysis (sensitivity of 0.46 and 0.92 for PET and MRI, respectively). However, DCFBC PET was more specific than MRI by per-segment analysis (specificity of 0.96 and 0.89 for PET and MRI for corresponding sensitivity, respectively) and specific for detection of high-grade lesions (Gleason 8 and 9) greater than 1.0 mL in size (4 of 4 of these patients positive by PET). DCFBC uptake in tumors was positively correlated with Gleason score ($\rho = 0.64$, PSMA expression ($\rho = 0.47$) and PSA ($\rho = 0.52$). There was significantly lower DCFBC uptake in benign prostatic hypertrophy (BPH) compared to primary tumors (median SUV_{max} 2.2 versus SUV_{max} 3.5; $P = 0.004$).

Conclusions: Although the sensitivity of DCFBC for primary prostate cancer was less than MRI, DCFBC PET was able to detect the more clinically significant high-grade and larger volume tumors (Gleason score 8 and 9) with higher specificity than MRI. In particular, there was relatively low DCFBC PET uptake in BPH lesions compared to cancer in the prostate, which may allow for more specific detection of primary prostate cancer by DCFBC PET. This study demonstrates the utility of PSMA-based PET which may be used in conjunction with MRI to identify clinically significant prostate cancer..

Key Words: Primary prostate cancer, prostate specific membrane antigen (PSMA), PET/CT, MRI, prostatectomy.

ClinicalTrials.gov Identifier#: NCT01496157

INTRODUCTION

In the United States prostate cancer remains the most commonly diagnosed cancer and second leading cause of cancer-related death in men (*1*). Accurate detection and appropriate management of patients with suspected primary prostate cancer is both challenging and controversial from clinical and imaging perspectives (*2*). Differentiation of indolent, low-risk from aggressive, high-risk and potentially lethal disease at initial diagnosis represents an unmet clinical need. Development of new methods allowing appropriate risk stratification to conservative management, such as active surveillance programs, or definitive therapy, such as prostatectomy, radiotherapy, and/or up-front androgen-deprivation are necessary (*3*). Incorporation of imaging to current primary prostate cancer classifications for risk stratification can help achieve that unmet clinical need.

Multi-parametric prostate MRI, by combining anatomic and functional information, is emerging as an accurate tool for detection of primary prostate cancer compared to the traditional, 12-core random, trans-rectal ultrasound-guided technique, particularly in its ability to detect such aggressive features as capsular and seminal vesicle invasion (*4, 5*). However, MRI suffers from false positives in nodules of benign prostatic hyperplasia (BPH), which can have an imaging appearance that overlaps with prostate adenocarcinoma (*6*). Furthermore, small foci of disease, low grade disease, and disease within the central gland may all be occult with MRI (*5*).

PET imaging has become an important functional imaging tool for diagnosis and staging in oncology, and a number of PET radiotracers have been developed and are being evaluated for detection and localization of primary prostate cancer (*7, 8*). ^{18}F-FDG is generally limited for the detection of primary prostate cancer. Other PET radiotracers evaluated for detection of primary

prostate cancer include various agents targeting fatty acid metabolism (^{11}C-choline, ^{18}F-choline, ^{11}C-acetate) (*9-12*) and amino acid transport (anti-1-amino-3-^{18}F-fluorocyclobutane-1-carboxylic acid, or ^{18}F-FACBC) (*13, 14*). Those radiotracers are able to demonstrate increased PET uptake at sites of primary prostate cancer compared to normal prostate tissue but generally have limited specificity for differentiating malignant from non-malignant processes, such as BPH and prostatitis, and have low sensitivity for small tumors. Additional new PET radiotracers are being developed, including small-molecules that target the prostate-specific membrane antigen (PSMA), gastrin-releasing peptide receptor (GRPR), and glutamine, all of which show promise for imaging prostate cancer but have not been systematically evaluated for detection of primary disease (*15-18*).

PSMA is a rational and promising target for imaging prostate cancer given its high expression in this disease. Expression in primary and metastatic lesions is associated with tumor grade and clinical outcome (*19-21*). We have previously demonstrated the ability of N-[N-[(*S*)-1,3-dicarboxypropyl]carbamoyl]-4-[^{18}F]fluorobenzyl-L-cysteine (DCFBC, Figure 1) to bind to prostate tumors with high PSMA expression in preclinical studies (*22*), as well as in a first-in-man study, to localize prostate metastases to both bone and soft tissue accurately (*23*). In this prospective study, we further evaluated DCFBC PET for detection and characterization of primary prostate cancer in men undergoing definitive surgery with correlation to pelvic magnetic resonance imaging (MRI) and pathology post-prostatectomy.

MATERIALS AND METHODS

Patient Population and Selection

All studies were performed in accordance with the Johns Hopkins University Institutional Review Board under a Food and Drug Administration exploratory investigational new drug application (eIND 108943). Written, informed consent was obtained from all patients. Pertinent inclusion criteria for this study included newly diagnosed patients with biopsy proven prostate cancer with Gleason score ≥ 6, considered as candidates for and medically fit to undergo prostatectomy, and at least 10 days after the most recent prostate biopsy at the time of PET imaging. Pertinent exclusion criteria included prior history of any other malignancy within last 2 years other than skin basal cell or nonmetastatic cutaneous superficial squamous cell carcinoma and superficial bladder cancer, history of prior radiation or systemic therapy for prostate cancer, renal dysfunction with serum creatinine > 1.5 mg/dL or creatinine clearance < 50 mL/min/1.73 m^2, and prostatectomy scheduled prior to a follow-up call that occurred within 12 to 72 hours post-imaging.

Fifteen patients were prospectively enrolled between September, 2012 and April, 2014. Thirteen patients were imaged with DCFBC PET/CT, with 12 of these patients also imaged with a pelvic prostate MRI (one patient was unable to undergo MRI due to a previously undisclosed remote history of foreign metal object). Two patients were enrolled but dropped out prior to any study-related DCFBC administration or imaging.

Radiochemistry

2-[3-(1-Carboxy-2-mercapto-ethyl)-ureido]-pentanedioic acid was prepared as previously described (*24*). Non-radiolabeled DCFBC precursors and standard were prepared according to a modification of a literature procedure to conform to current good manufacturing practice (*25*).

DCFBC was prepared as previously published (*23, 26*). The specific activity range of administered DCFBC was 62.9 - 2084 GBq/μmole (1699 - 56318 mCi/μmole) with a median of 335 GBq/μmole (9059 mCi/μmole). The variation in specific activity at time of injection may have been due in part to one or more of the following: starting amounts of ^{18}F-fluoride, carrier fluoride in target water, transfer tubings, and valves, minute and variable UV absorbing components from different batches of saline in the radiotracer product matrix used over the course of the study, and the interval between the end of synthesis and the time of injection (i.e., subject preparation and scanner availability).

PET/CT Protocol

Patients were instructed to be *nil per os* (except for water and some medications) for at least six hours prior to the administration of DCFBC. Patients were specifically asked not to take multi-vitamins and folic acid supplements on the day of the examination because folate is a substrate for PSMA and high folate levels can potentially reduce DCFBC binding (*15, 27*). Serum folate was obtained prior to DCFBC administration. A coudé catheter was placed in the urinary bladder as tolerated, which allowed for consistent placement for both PET and MRI in these patients to allow for improved PET and MRI co-registration.

PET/CT was performed on a Discovery DRX PET/CT scanner (GE Healthcare, Waukesha, WI) operating in 2D and 3D emission acquisition mode with CT for attenuation correction. Scans were performed with patients in the supine position. A bolus of 10 ± 1 mCi (370 ± 37 MBq) of DCFBC was injected by slow IV push. Two hours post-injection, a CT of the pelvis was obtained [120 kVp, 80 mA maximum (auto-adjusting)] followed by a 30-minute

dynamic list-mode 2D PET emission acquisition, then an additional five minute pelvic 3D PET, both with the prostate in the center of the field-of-view. 2D PET acquisition mode was used for this pelvic PET imaging in order to minimize potential scatter causing a PET quantitation artifact from the high urinary radioactivity in the bladder. A total of six, 5-minute frames were reconstructed with a high-resolution filter and summed to produce the 2D pelvic PET images. Pelvic PET images were acquired on a flat table with arms raised in order to allow for optimal co-registration with the corresponding MRI images. Following completion of the dynamic pelvic PET/CT scans at approximately 2.5 hours post-injection, a whole body (WB) PET/CT was acquired from the vertex of the skull through the mid-thigh in 3D mode for 4 minutes and 15 seconds at each bed position. All PET images were reconstructed using a standard clinical ordered subset expectation maximization (OSEM) algorithm.

MRI Acquisition

All pelvic MRI studies were obtained on the same day as the PET acquisitions except for one patient imaged nine days later. MRI studies were performed on a 3T whole body TRIO scanner with a TIM body matrix coil (Siemens Medical Solutions, Malvern, PA, USA). The sequences acquired included thin-section high-resolution axial, coronal, and sagittal T2-weighted fast spin echo (FSE), diffusion weighted imaging (DWI) with corresponding apparent diffusion coefficient (ADC) maps from a 2D multi-slice single-shot diffusion-weighted echo planar (EP) sequence, and a single-slab 3D isometric T2-weighted turbo spine echo sequence (SPACE or sampling perfection with application-optimized contrast using different flip angle evolution). The 3D T2-weighted SPACE sequence was acquired to allow high fidelity co-registration with

the PET and CT images given that its isometric voxels could be reconstructed in any needed plane. Axial T1 non-contrast images were obtained using a gradient echo technique with low flip angles (FLASH or fast low angle shot). No gadolinium contrast enhanced imaging was acquired as the T1 sequence was primarily used to identify areas of hemorrhage.

Image Analysis

Three experienced nuclear medicine readers (SYC, KLG, and SPR), who were blinded to the MRI and histopathologic results, reached a consensus determination on DCFBC uptake within the prostate on both a lesion and sector basis. Visual analysis was used to define focal DCFBC uptake as being above background activity in the prostate and blood pool in the peri-prostatic vascular plexus. For the subsequent analysis, foci of uptake were defined on a 3-point scale as 1 = negative, 2 = equivocal, or 3 = positive. PET maximum standarized uptake values (SUV_{max}) corrected for lean body mass were calculated for the foci of PET uptake in the prostate on the 2D pelvis, 3D pelvis, and WB PET acquisitions using Mirada Medical XD Software (Oxford, United Kingdom). For sites of prostate tumors seen on pathology that were occult on PET, a tumor SUV_{max} was obtained using a representative spherical 1 cm diameter volume of interest (VOI) placed in the approximate tumor location on each PET acquisition, using the prostatectomy specimen as a guide. To evaluate uptake in BPH, the axial T2-weighted MR images were virtually fused to each of the 2D pelvis, 3D pelvis, and WB PET acquisitions using rigid registration with the femoral heads as fiducial markers on the Mirada Medical workstation. Ellipsoid VOIs corresponding to the T2 signal abnormalities deemed to be representative of BPH on the MR images were then drawn and the SUV_{max} for each focus of BPH was determined.

Care was taken in drawing the VOI of all cases of both tumor and BPH to avoid including any of the high radioactivity in the urinary bladder.

An experienced reader of prostate MR images (KM), who was similarly blinded to the PET/CT and histopathologic results, evaluated the MR images. From a multi-parametric visual analysis including diffusion weighted imaging and high resolution T1 and T2 imaging, a sector-based determination of the presence of cancer, hemorrhage, BPH, and prostatitis was performed. Lesion-based analysis for the presence of cancer was also performed. Potential sites of cancer were subjectively graded on a 5-point scale (1 = highly unlikely to be cancer, 2 = unlikely to be cancer, 3 = equivocal, 4 = likely to be cancer, 5 = highly likely to be cancer).

Histopathologic Analysis

All 13 patients that participated in the imaging portion of the study proceeded to have radical prostatectomy with lymph node dissection as is standard of surgical care at our institution. Briefly, prostate specimens were injected with formalin. Nine were subsequently microwave-fixed and four were fixed in formalin overnight. Following fixation, the external surface was differentially inked to indicate the surgical margins per our laboratory standard protocol. The prostatectomy specimens were axially serially sectioned at 4-mm intervals after the proximal and the distal margins and seminal vesicles were removed and entirely submitted for histologic examination. All prostate slices were photographed with a ruler, labeled, and then quartered to produce right anterior, left anterior, right posterior, and left posterior segments; in combination with the base, mid, and apex designations, this method of sectioning the gland provided the basis for the 12-segment model used extensively for lesion localization.

The prostate tissue fragments were embedded in paraffin and stained with hematoxylin-eosin (HE) using standard methods. Expert urologic pathologist (GJN in consensus with GG, SFF or EM) reviewed the slides and noted the presence of any prostate cancer, Gleason grades, and the size of the tumors. A representative section from the dominant (index) nodule in each prostatectomy specimen was selected for immunohistochemical analysis. The dominant nodule was defined as the nodule with the highest Gleason score tumor, which in the large majority of cases was also the largest in size. If a higher Gleason grade was noted in a smaller nodule, that smaller nodule was considered the dominant.

The representative sections from the dominant (index) tumor nodule were then analyzed by immunohistochemical (IHC) methods for expression of PSMA, prostate specific antigen (PSA), ERG, and Ki-67. Appropriate internal and external controls were also processed and assessed in parallel. An H-score was assigned as the sum of the products of the intensity (0 for negative, 1 for weakly positive, 2 for moderately positive, and 3 for strongly positive) multiplied by the extent of expression (0% to 100%), obtaining a value ranging from 0 to 300 (*28*). The presence of Ki-67 was reported as a percentage of the tumor cells that demonstrated positive staining. Modified H-scores were calculated for PSMA taking into account only the strong and moderate staining portions of the tumor ($\text{H-score}_{\text{mod-str}}$ = [(percentage of tumor strongly staining x 3) + (percentage of tumor moderately staining x 2)]) or only the strong staining portions of the tumor ($\text{H-score}_{\text{str}}$ = [percentage of tumor strongly staining x 3]). The PSMA H-scores (including $\text{H-score}_{\text{mod-str}}$ and $\text{H-score}_{\text{str}}$) were also multiplied by the dominant nodule volumes to provide additional metrics designated by [H-score x volume].

Correlation between Histopathology and Imaging

HE slides were scanned at 20x using iScan Coreo (Ventana, Tucson, AZ). Photoshop CS6 (Adobe Systems, San Jose, California) was used to manually reassemble the prostate quarters into full slices and to register the histology sections to the gross photographs. For each reassembled slice, outlines of tumor, urethra and prostate gland were then created as layers in Photoshop.

Correlation between histology and the imaging modalities was performed on a per-segment and per-lesion basis. First, the 12-segment prostate model was utilized, designating each segment containing prostate cancer determined at pathology. Each suspicious finding previously noted on DCFBC PET and prostate MRI interpretation was assigned to one or more contiguous segments depending on its location and extent. Additionally, BPH and hemorrhage identified on MRI were assigned to segments in which they were present. In that particular set of patients, mild diffuse T2 signal hypointensity within the prostate that might have indicated prostatitis was not observed. Furthermore, a lesion-based correlation was performed between the dominant tumor on pathology, the corresponding uptake on DCFBC PET, and detection by MRI signal abnormality.

Statistical Analysis

Utilizing the 12-segment model described above, the sensitivity, specificity, positive predictive value (PPV), negative predictive value (NPV), and overall accuracy of DCFBC PET/CT and multi-parametric MRI were calculated using HE as the reference standard. Those values were determined with both non-stringent and stringent reading of the imaging modalities,

with non-stringent reading defined with equivocal findings (2 on PET, 3 on MRI) considered to be positive and stringent reading defined with equivocal findings as negative. For that analysis, 1 and 2 on the 5-point scale were considered negative on MRI. Estimates of sensitivity, specificity, PPV, NPV, overall accuracy and their corresponding 95% confidence limits were derived from intercept-only generalized estimating equation (GEE) regression models. The same 12-segment model was used to correlate findings of hemorrhage and BPH between PET and MRI using a logistic regression model estimated via a GEE to arrive at between-group differences. Sensitivity of PET and MRI for the detection of the dominant nodule in each patient was also determined on both a non-stringent and stringent basis.

A number of additional correlations were drawn between PET and MRI imaging parameters and the pathologic findings. Those included the various PSMA H-score and [H-score x volume] metrics versus 2D pelvis, 3D pelvis, and WB PET SUV_{max} PSMA H-score and H-score x volume metrics versus MRI ADC values; and PET SUV_{max} versus MRI ADC values. Nonparametric Pearson correlation coefficients were calculated to describe associations.

Further analysis was performed with uptake in BPH in comparison to the visually positive tumors, both non-stringently and stringently assessed. GEE regression analysis was utilized to determine between-group differences in the PET uptake among BPH and the visually positive tumors.

RESULTS

Table 1 includes selected demographic information for the 13 patients recruited. The average age was 62 years (with a standard deviation of 6 years and a range from 54 years through 71 years). The most recent available PSA values at the time of the DCFBC PET/CT

scan are also noted, with average of 8.4 ng/mL (with a standard deviation of 3.8 ng/mL and range from 5.3 ng/mL through 17.0 ng/mL).

A 12-segment prostate analysis for cancer detection with both PET and MRI compared to histology at prostatectomy for tumor is summarized in Table 2, including non-stringent (rows 1 and 3) and stringent (rows 2 and 4) image analyses. Of note, neither DCFBC PET nor MRI demonstrated high sensitivity for cancer detection (sensitivities of 0.17 and 0.39 for PET and MRI for non-stringent analysis and 0.10 and 0.35 for stringent analysis, respectively), likely reflecting the ability of the interpreting pathologists to identify small to microscopic amounts of tumor in many segments that would be occult on any imaging modality. While overall accuracy for both modalities using the 12-segment analysis was modest, both DCFBC PET and MRI demonstrated high specificity and positive-predictive value (PPV) for segment-based prostate cancer detection (specificity of 0.96 and 0.89 for PET and MRI, respectively, for non-stringent analysis). There was a trend towards DCFBC PET being marginally more specific than MRI in this portion of the analysis (0.96 versus 0.89 for non-stringent analysis and 1.00 versus 0.91 for stringent analysis, respectively).

In a lesion-based analysis of dominant (index) primary prostate tumor, both modalities had improved sensitivity compared to the 12-segment analysis, as seen in Table 3, although MRI had an increased sensitivity compared to DCFBC PET. Specificity was not calculated due to small sample size of the dominant lesions. The gap in lesion sensitivity between the two modalities decreased when the analysis was limited to only Gleason 8 and 9 cancers (MRI: 1.00 non-stringent and 0.80 stringent; PET 0.80 non-stringent and 0.60 stringent). As expected, the sensitivities of both modalities trended lower when equivocal findings were considered negative. Interestingly, the detection of dominant lesions with DCFBC PET was not solely dependent on

tumor size, as would be of concern for any modality in which partial volume effects can obscure small lesions. Table 4 shows that primary prostate tumor size and Gleason score must both influence lesion detectability by DCFBC PET as seen by an undetectable Gleason 7 tumor greater than 5 mL in volume and positive uptake in a smaller 1.1 mL Gleason 9 lesion. Tumors less than 1.1 mL and Gleason 4+3=7 were limited in detection by PET, likely in part due to small size and in part to low PSMA expression. On a per-patient basis, as per Table 4, 6 of 13 patients were DCFBC PET positive (4 positive on stringent and 6 positive on non-stringent PET reads). All 4 of 4 patients with high grade (Gleason 8 and 9) and large volume dominant lesions (>1.0 mL) were detectable by PET. However, two patients with low-volume (<1.0 mL) Gleason 4+4=8 and 4+3=7 disease and others with lower grade Gleason grade tumors were not detectable by DCFBC PET. Figure 2 shows an example of PET and MRI imaging of primary prostate cancer in a patient with a Gleason 9 tumor with corresponding pathology and demonstration of high tumor PSMA expression.

Our original rationale to acquire 2D and 3D pelvic PET images, as well as later WB 3D PET acquisition, was to control for the possibility of increased scatter from the urinary bladder radioactivity into the adjacent prostate gland on 2D compared to 3D images. However, that phenomenon was not observed to any measurable extent visually or quantitatively, as seen in Table 5. Visually, the later WB images demonstrated the highest tumor-to-background normal prostate and blood pool uptake with improved lesion conspicuity, most likely as a result of their later acquisition time, which allowed some background blood pool radioactivity to clear with respect to DCFBC-mediated radioactivity within tumor (Table 5). DCFBC PET tumor to blood pool ratio (Tumor SUV_{max}/Blood pool SUV_{mean}) using the right common femoral vein for blood pool demonstrate this trend of increasing tumor to background ratio on later whole body PET

acquisitions (Supplemental Figure 1). Given those considerations, we chose to perform all subsequent analyses using the SUVs derived from the whole-body PET acquisitions obtained at the longest duration after DCFBC injection, unless otherwise specified (time interval of approximately 2.5 hours post-injection). Notably there were no incidental findings on the whole-body PET images in any patients to suggest metastatic disease.

In reviewing the data from the three different PET acquisitions (2D pelvis, 3D pelvis, and whole-body), it was observed that there was a statistically significant positive correlation ($P<0.05$) between the Gleason scores of the tumors and the obtained maximum SUVs for all three acquisitions (Figure 3). We observed nearly no relationship between Gleason score and ADC values in our study (Supplemental Figure 2). When correlating SUV_{max} to PSMA expression (PSMA H-score, PSMA H-score$_{mod-str}$, and PSMA H-score$_{str}$), positive relationships were noted for all three PSMA IHC scores with a trend towards but no statistical significance (Supplemental Figure 3, ρ values between 0.31 and 0.51; P value of 0.1, 0.07, 0.3, respectively). In regards to non-PSMA IHC findings, we observed a positive correlation between PSA H-score and SUV_{max}, a negative correlation between ERG H-score and SUV_{max} (ρ -0.31), and a negative correlation between Ki-67 staining and SUV_{max} (ρ -0.28) (Supplemental Figure 3); none of these associations reached statistical significance. (More details on these correlations, as well as correlation of MRI ADC to IHC parameters, are presented in the supplemental data section.)

Figure 4 shows the relative photopenia we observed in BPH compared to the rest of the prostate gland. The central gland is noted to have two large BPH nodules (arrowheads). BPH does not express PSMA and does not demonstrate focal uptake with DCFBC. Across all of the imaged BPH lesions and PET-positive tumors, there is a statistically significant difference in

uptake between BPH and PET positive prostate cancers (Figure 5, $P = 0.004$ and 0.016, respectively).

DISCUSSION

Major considerations in the management of prostate cancer is accurate initial diagnosis and distinguishing aggressive from indolent disease for selection of appropriate therapy. Patient care initially requires accurate tumor evaluation in order to select the optimal therapy from a growing array of alternatives that include active surveillance, androgen ablation, radical prostatectomy (radical retropubic or laparoscopic/robotic), radiation therapy (brachytherapy, external-beam radiation therapy, or combinations of these choices), and possibly focal ablative therapies (cryoablation, radiofrequency ablation, brachytherapy, laser ablation and focused ultrasound) (*3, 29, 30*). Patients are risk-stratified based on serum PSA level, tumor grade, and clinical stage, with predictive models having been developed to determine pathologic stage and time to recurrence based on retrospective patient data (*31*). However, those outcome models, while effective, do not adequately identify all patients at risk of developing biochemical recurrence and provide no anatomical localization of tumor spread (*32*).

The combined anatomic and functional imaging provided by PET suggests that a PET radiotracer for the proper target may dramatically improve imaging of prostate cancer. Studies with FDG, the most commonly used clinical PET radiotracer, have demonstrated low uptake in prostate cancer except for advanced metastatic disease (*33, 34*). However, a number of new radiotracers for prostate cancer are in various stages of development as noted in the introduction. In particular, choline, acetate and ^{18}F-FACBC PET imaging have been hampered by decreased

specificity in differentiating malignant from benign hyperplastic prostatic lesions (*11, 12, 14*), although the PET radiotracer synthetic bombesin receptor antagonist for GRP was able to differentiate between malignant and benign hyperplastic prostate lesions (*18*).

PSMA is a promising, well-characterized biomarker specific for prostate cancer, which has also been associated with prostate tumor aggressiveness. Histologic studies have associated high PSMA expression with metastatic spread (*35-37*), androgen independence (*38*), and expression levels have been found to be predictive of prostate cancer progression (*19, 21*).

Our prospective study evaluated the utility of DCFBC, a small-molecule PSMA inhibitor, for the detection of primary prostate cancer. We were able to detect clinically significant high grade (Gleason 8 and 9) and larger sized (≥ 1.1 mL) primary prostate tumors reliably, with no evidence of uptake in BPH. DCFBC PET was however limited for detection of smaller sized (< 1.1 mL) and lower grade (Gleason 7 or 6) tumors. Although low-grade tumors were found to have variable and generally low level uptake, there was nevertheless a positive correlation between DCBFC uptake, as measured by SUV_{max} and Gleason score of the prostate cancers included in this trial. We have observed a trend towards a positive correlation between DCFBC PET tumor uptake compared to PSMA tumor expression by IHC, although a study with larger sample size is needed to confirm these preliminary results. MRI demonstrated greater sensitivity for the detection of prostate cancer, but can oftentimes reveal multiple lesions whereas DCFBC PET can potentially allow for more specific localization of the highest-grade and most clinically significant lesion.

This study had several limitations. First, the overall detection rate of prostate cancer by DCFBC PET/CT in our patient cohort was lower than multi-parametric MRI, although the

detection rate improved with higher grade tumors (Gleason 8 and 9). We were limited by the accrual pattern of patients that entered our study having predominantly low-grade tumors (Gleason 6 and 7), which are known to have relatively low PSMA expression levels (*19, 21*). Attempting to include more patients with tumors of higher Gleason grade in the initial recruitment process would likely have improved our rate of detection. Another important consideration is that many tumors in the prostate are small (significantly less than 1 cm in diameter), rendering them susceptible to partial volume effects. However, when correcting for lesion size we showed that the detection of dominant lesions with DCFBC PET was not solely dependent on tumor size but also involved tumor PSMA expression. It is likely that small tumors may have been volume-averaged with surrounding normal prostate tissue preventing their detection on PET imaging in patients with low-grade tumors and corresponding low levels of PSMA expression.

Another consideration arises from the intrinsic properties of DCFBC. DCFBC is a first-generation ^{18}F-labeled agent that demonstrated high and specific uptake in PSMA-expressing experimental models and in patients with metastatic disease (*22, 23*). DCFBC tends to persist in the blood pool, likely secondary to plasma protein binding, which limits optimal clearance from soft tissue and diminishing tumor-to-background ratio and detection of lower avidity and/or smaller lesions. ^{68}Ga-PSMA (*39*) and a new second-generation ^{18}F-PSMA-targeted agent (^{18}F-DCFPyL) (*40*) demonstrate high tumor uptake with lower-background which promises improved signal for better detection of lower-grade and/or smaller sized primary prostate tumors compared to DCFBC. It is important to note that the low DCFBC PET uptake in BPH shown in this study demonstrates that these emerging PSMA-based PET imaging agents can also potentially greatly improve the specificity for differentiating benign hyperplastic from malignant prostate lesions,

which has also been an important reported feature of a new GRPR radiopharmaceutical (*18*), but a limitation of acetate, choline and ^{18}F-FACBC PET imaging for this application (*11, 12, 14*).

CONCLUSION

DCFBC PET can detect clinically significant, high-grade prostate cancer and shows promise for differentiating malignant prostate cancer from non-malignant prostate lesions such as BPH. With further validation, PSMA-targeted PET imaging, in conjunction with MRI, may allow for directed biopsy of the most clinically significant lesions and function as a non-invasive imaging biomarker for differentiating indolent versus aggressive disease, thus improving risk-adaptive management.

DISCLOSURES

None.

ACKNOWLEDGMENTS

We thank the Prostate Cancer Foundation (PCF) and Movember for the PCF Creativity Award, the Brady Patana Research Fund, EB006351, and CA134675 for funding. We also thank Akimosa Jeffrey-Kwanisai and Yavette Morton for their dedication to, and clinical coordination of, this trial.

REFERENCES

1. Siegel R, Ma J, Zou Z, Jemal A. Cancer statistics, 2014. *CA Cancer J Clin.* 2014;64:9-29.

2. Cuzick J, Thorat MA, Andriole G, et al. Prevention and early detection of prostate cancer. *Lancet Oncol.* 2014;15:e484-e492.

3. Chang AJ, Autio KA, Roach M, 3rd, Scher HI. High-risk prostate cancer-classification and therapy. *Nat Rev Clin Oncol.* 2014;11:308-323.

4. Johnson LM, Turkbey B, Figg WD, Choyke PL. Multiparametric MRI in prostate cancer management. *Nat Rev Clin Oncol.* 2014;11:346-353.

5. Dianat SS, Carter HB, Macura KJ. Performance of multiparametric magnetic resonance imaging in the evaluation and management of clinically low-risk prostate cancer. *Urol Oncol.* 2014;32:39 e31-10.

6. Bonekamp D, Jacobs MA, El-Khouli R, Stoianovici D, Macura KJ. Advancements in MR imaging of the prostate: from diagnosis to interventions. *Radiographics.* 2011;31:677-703.

7. Kiess AP, Cho SY, Pomper MG. Translational Molecular Imaging of Prostate Cancer. *Curr Radiol Rep.* 2013;1:216-226.

8. Jadvar H. Molecular imaging of prostate cancer with PET. *J Nucl Med.* 2013;54:1685-1688.

9. Farsad M, Schiavina R, Castellucci P, et al. Detection and localization of prostate cancer: correlation of (11)C-choline PET/CT with histopathologic step-section analysis. *J Nucl Med.* 2005;46:1642-1649.

10. Kwee SA, Thibault GP, Stack RS, Coel MN, Furusato B, Sesterhenn IA. Use of step-section histopathology to evaluate 18F-fluorocholine PET sextant localization of prostate cancer. *Mol Imaging.* 2008;7:12-20.

11. Mena E, Turkbey B, Mani H, et al. 11C-Acetate PET/CT in localized prostate cancer: a study with MRI and histopathologic correlation. *J Nucl Med.* 2012;53:538-545.

12. Souvatzoglou M, Weirich G, Schwarzenboeck S, et al. The sensitivity of [11C]choline PET/CT to localize prostate cancer depends on the tumor configuration. *Clin Cancer Res.* 2011;17:3751-3759.

13. Schuster DM, Taleghani PA, Nieh PT, et al. Characterization of primary prostate carcinoma by anti-1-amino-2-[(18)F] -fluorocyclobutane-1-carboxylic acid (anti-3-[(18)F] FACBC) uptake. *Am J Nucl Med Mol Imaging.* 2013;3:85-96.

14. Turkbey B, Mena E, Shih J, et al. Localized prostate cancer detection with 18F FACBC PET/CT: comparison with MR imaging and histopathologic analysis. *Radiology.* 2014;270:849-856.

15. Foss CA, Mease RC, Cho SY, Kim HJ, Pomper MG. GCPII imaging and cancer. *Curr Med Chem.* 2012;19:1346-1359.

16. Huang C, McConathy J. Fluorine-18 labeled amino acids for oncologic imaging with positron emission tomography. *Curr Top Med Chem.* 2013;13:871-891.

17. Wieser G, Mansi R, Grosu AL, et al. Positron emission tomography (PET) imaging of prostate cancer with a gastrin releasing peptide receptor antagonist--from mice to men. *Theranostics.* 2014;4:412-419.

18. Kahkonen E, Jambor I, Kemppainen J, et al. In vivo imaging of prostate cancer using [68Ga]-labeled bombesin analog BAY86-7548. *Clin Cancer Res.* 2013;19:5434-5443.

19. Ross JS, Sheehan CE, Fisher HA, et al. Correlation of primary tumor prostate-specific membrane antigen expression with disease recurrence in prostate cancer. *Clin Cancer Res.* 2003;9:6357-6362.

20. Marchal C, Redondo M, Padilla M, et al. Expression of prostate specific membrane antigen (PSMA) in prostatic adenocarcinoma and prostatic intraepithelial neoplasia. *Histol Histopathol.* 2004;19:715-718.

21. Perner S, Hofer MD, Kim R, et al. Prostate-specific membrane antigen expression as a predictor of prostate cancer progression. *Hum Pathol.* 2007;38:696-701.

22. Foss CA, Mease RC, Fan H, et al. Radiolabeled small-molecule ligands for prostate-specific membrane antigen: in vivo imaging in experimental models of prostate cancer. *Clin Cancer Res.* 2005;11:4022-4028.

23. Cho SY, Gage KL, Mease RC, et al. Biodistribution, Tumor Detection, and Radiation Dosimetry of 18F-DCFBC, a Low-Molecular-Weight Inhibitor of Prostate-Specific Membrane Antigen, in Patients with Metastatic Prostate Cancer. *J Nucl Med.* 2012;53:1883-1891.

24. Kozikowski AP, Nan F, Conti P, et al. Design of remarkably simple, yet potent urea-based inhibitors of glutamate carboxypeptidase II (NAALADase). *J Med Chem.* 2001;44:298-301.

25. Mease RC, Dusich CL, Foss CA, et al. N-[N-[(S)-1,3-Dicarboxypropyl]carbamoyl]-4-[18F]fluorobenzyl-L-cysteine, [18F]DCFBC: a new imaging probe for prostate cancer. *Clin Cancer Res.* 2008;14:3036-3043.

26. Holt DP RH, Mathews WB, Horti A, Mease R, Dannals RF. A semi-automated microwave chemistry system for complete radiosynthesis, purification, and formulation of F-18 radiotracers. *J Label Compd Radiopharm.* 2011;54.

27. Yao V, Berkman CE, Choi JK, O'Keefe DS, Bacich DJ. Expression of prostate-specific membrane antigen (PSMA), increases cell folate uptake and proliferation and suggests a novel role for PSMA in the uptake of the non-polyglutamated folate, folic acid. *Prostate.* 2010;70:305-316.

28. Chaux A, Albadine R, Toubaji A, et al. Immunohistochemistry for ERG expression as a surrogate for TMPRSS2-ERG fusion detection in prostatic adenocarcinomas. *Am J Surg Pathol.* 2011;35:1014-1020.

29. Sartor O, Eisenberger M, Kattan MW, Tombal B, Lecouvet F. Unmet needs in the prediction and detection of metastases in prostate cancer. *Oncologist.* 2013;18:549-557.

30. Walsh PC, DeWeese TL, Eisenberger MA. Clinical practice. Localized prostate cancer. *N Engl J Med.* 2007;357:2696-2705.

31. Han M, Partin AW, Zahurak M, Piantadosi S, Epstein JI, Walsh PC. Biochemical (prostate specific antigen) recurrence probability following radical prostatectomy for clinically localized prostate cancer. *J Urol.* 2003;169:517-523.

32. Cowen ME, Halasyamani LK, Kattan MW. Predicting life expectancy in men with clinically localized prostate cancer. *J Urol.* 2006;175:99-103.

33. Turlakow A, Larson SM, Coakley F, et al. Local detection of prostate cancer by positron emission tomography with 2-fluorodeoxyglucose: comparison of filtered back projection and iterative reconstruction with segmented attenuation correction. *Q J Nucl Med.* 2001;45:235-244.

34. Hofer C, Laubenbacher C, Block T, Breul J, Hartung R, Schwaiger M. Fluorine-18-fluorodeoxyglucose positron emission tomography is useless for the detection of local recurrence after radical prostatectomy. *Eur Urol.* 1999;36:31-35.

35. Bostwick DG, Pacelli A, Blute M, Roche P, Murphy GP. Prostate specific membrane antigen expression in prostatic intraepithelial neoplasia and adenocarcinoma: a study of 184 cases. *Cancer.* 1998;82:2256-2261.

36. Chang SS, Reuter VE, Heston WD, Gaudin PB. Comparison of anti-prostate-specific membrane antigen antibodies and other immunomarkers in metastatic prostate carcinoma. *Urology.* 2001;57:1179-1183.

37. Sweat SD, Pacelli A, Murphy GP, Bostwick DG. Prostate-specific membrane antigen expression is greatest in prostate adenocarcinoma and lymph node metastases. *Urology.* 1998;52:637-640.

38. Wright GL, Jr., Grob BM, Haley C, et al. Upregulation of prostate-specific membrane antigen after androgen-deprivation therapy. *Urology.* 1996;48:326-334.

39. Afshar-Oromieh A, Malcher A, Eder M, et al. PET imaging with a [68Ga]gallium-labelled PSMA ligand for the diagnosis of prostate cancer: biodistribution in humans and first evaluation of tumour lesions. *Eur J Nucl Med Mol Imaging.* 2013;40:486-495.

40. Szabo Z, Mena E, Rowe SP, et al. Initial Evaluation of [F]DCFPyL for Prostate-Specific Membrane Antigen (PSMA)-Targeted PET Imaging of Prostate Cancer. *Mol Imaging Biol.* 2015.

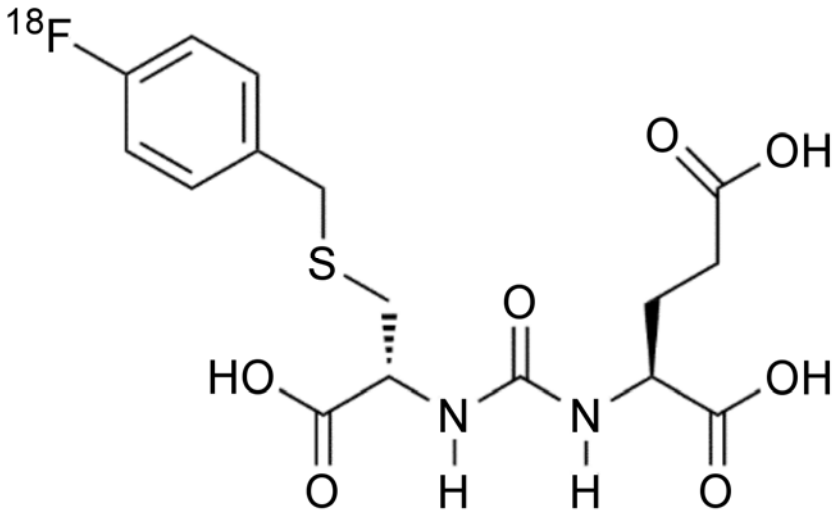

Figure 1 ^{18}F-DCFBC chemical structure

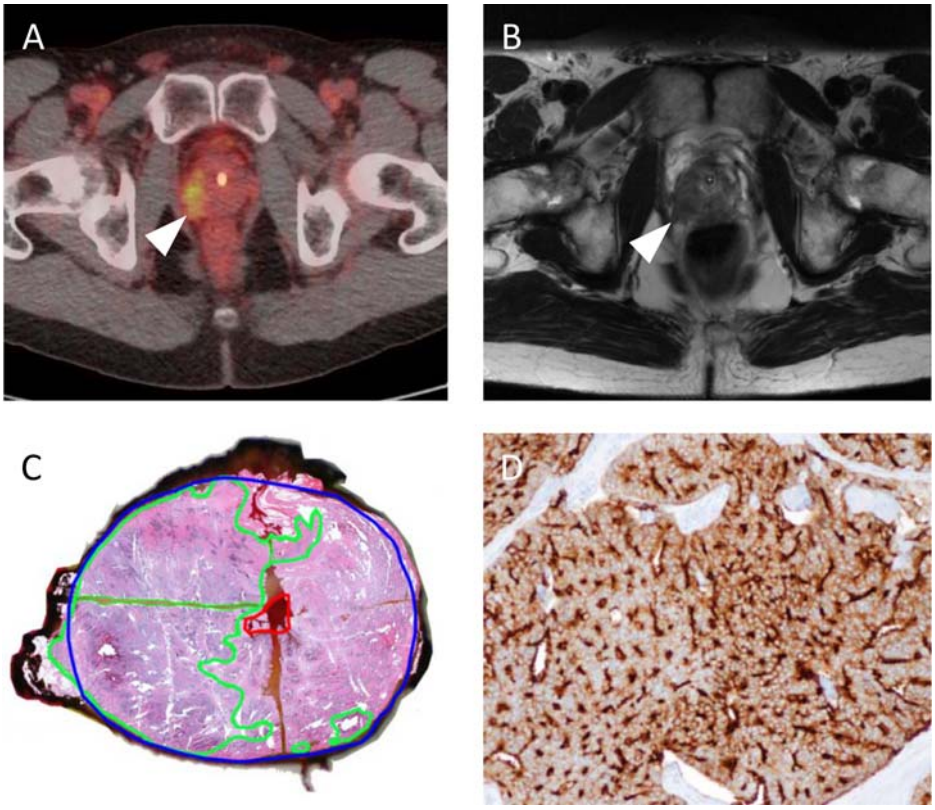

Figure 2 Correlation between focal uptake in the right lateral prostate apex on DCFBC PET (A), abnormal low T2 signal on MRI (B), and tumor on gross surgical pathology, as outlined in green (C). Pathologic specimen from the same tumor shows strong IHC staining for PSMA (brown color) (D).

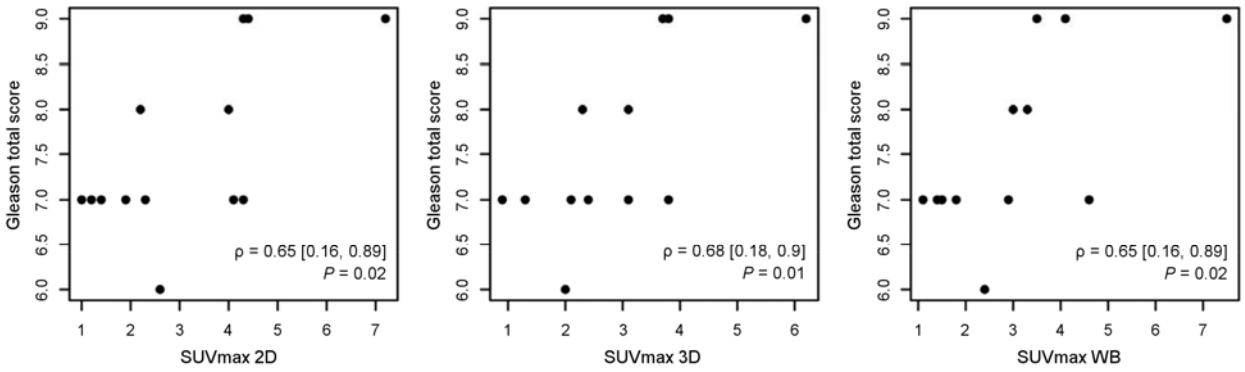

Figure 3 Scatter plot of DCFBC PET SUV_{max} and prostatectomy Gleason score for pelvic 2D, pelvic 3D, and WB PET acquisitions showing strong positive correlation.

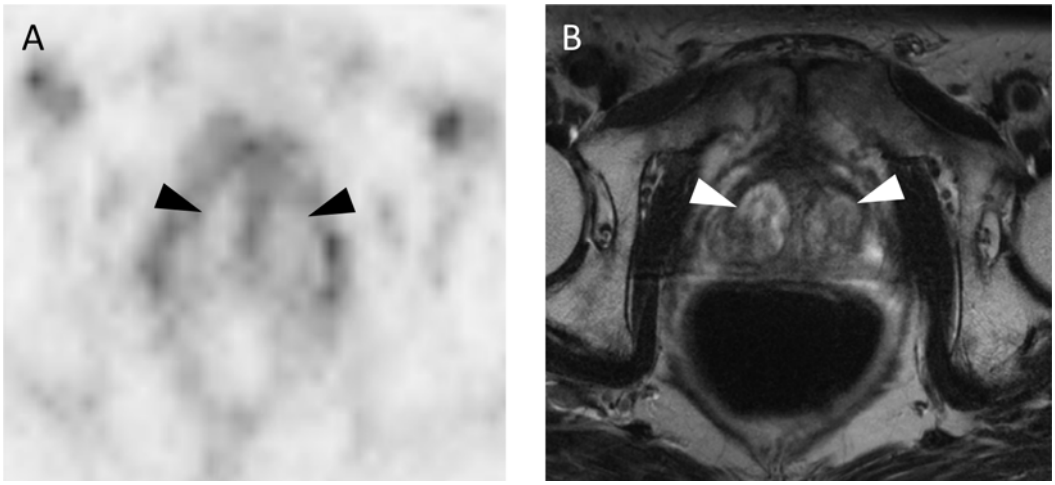

Figure 4 DCFBC PET (A) and T2-weighted MR (B) images demonstrating DCFBC photopenia for a representative example of BPH nodules within the central prostate.

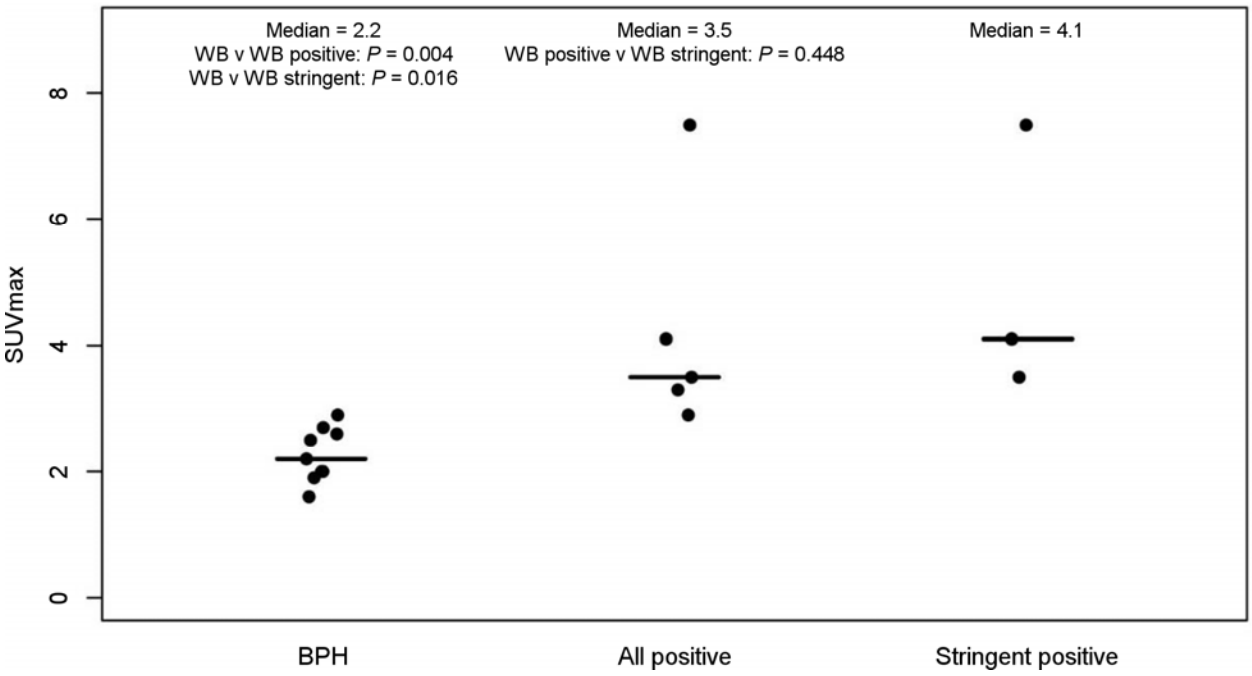

Figure 5 Plot showing ranges of SUV_{max} in BPH, all PET positive prostate cancers (non-stringent analysis), and tumors with PET positivity only in the stringent analysis.

Table 1.

Patient	Age	PSA (ng/mL)	Biopsy Gleason Score	Prostatectomy Gleason Score
1	58	5.7	3 + 3 = 6	3 + 3 = 6
2	71	17.0	4 + 4 = 8	4 + 5 = 9
3	65	4.5	4 + 3 = 7	4 + 3 = 7
4	54	5.3	3 + 4 = 7	3 + 4 = 7
5	55	13.9	4 + 4 = 8	4 + 5 = 9
6	57	5.6	4 + 3 = 7	4 + 5 = 9
7	61	10.5	3 + 4 = 7	3 + 4 = 7
8	61	9.1	4 + 3 = 7	4 + 3 = 7
9	71	6.8	3 + 4 = 7	3 + 4 = 7
10	66	8.5	3 + 4 = 7	3 + 4 = 7
11	59	5.8	4 + 3 = 7	5 + 3 = 8
12	62	10.5	3 + 4 = 7	3 + 4 = 7
13	70	5.5	4 + 4 = 8	4 + 4 = 8

Table 1 Patient Demographic and Clinical Information.

Table 2.

Modality	Sensitivity (95% CI)	Specificity (95% CI)	PPV (95% CI)	NPV (95% CI)	Accuracy (95% CI)
MRI - All positive	0.39 (0.25-0.54) N =69	0.89 (0.81-0.94) N = 75	0.73 (0.53-0.87) N = 34	0.58 (0.37-0.77) N = 110	0.65 (0.51-0.76) N = 144
MRI – Stringent	0.35 (0.20-0.55) N =69	0.91 (0.82-0.95) N = 75	0.73 (0.50-0.88) N = 29	0.58 (0.36-0.77) N = 115	0.62 (0.48-0.75) N = 144
DCFBC PET – All positive	0.17 (0.09-0.29) N = 77	0.96 (0.87-0.99) N = 79	0.81 (0.51-0.95) N = 16	0.53 (0.35-0.70) N = 140	0.57 (0.42-0.71) N = 156
DCFBC PET - Stringent	0.10 (0.04-0.25) N = 77	1.00 (1.00-1.00) N = 79	1.00 (1.00-1.00) N = 8	0.53 (0.35-0.70) N = 148	0.56 (0.39-0.71) N = 156

Table 2 PET and MRI Detection of Prostate Cancer on 12-segment Prostatectomy Pathology.

Table 3.

Modality	Sensitivity (95% CI)
MRI – All positive	0.92 (0.59-0.99), N = 12
MRI - Stringent	0.75 (0.45-0.92), N = 12
DCFBC PET – All positive	0.46 (0.22-0.72), N = 12
DCFBC PET - Stringent	0.23 (0.08-0.52), N = 13

Table 3 PET and MRI Dominant Pathology Lesion Detection Sensitivity.

Table 4.

Dominant Nodule Size (mL)	Patient	Prostatectomy Gleason Score	Visually Detected with DCFBC PET	SUV_{MAX}
8.92	13	4 + 4 = 8	Equivocal	3.3
7.07	5	4 + 5 = 9	Yes	3.5
5.48	12	3 + 4 = 7	No	1.7
4.86	7	3 + 4 = 7	Yes	4.6
2.41	2	4 + 5 = 9	Yes	4.1
1.23	9	3 + 4 = 7	No	1.4
1.12	6	4 + 5 = 9	Yes	7.5
0.73	11	5 + 3 = 8	No	2.3
0.56	10	3 + 4 = 7	No	1.9
0.49	1	3 + 3 = 6	No	2.4
0.44	3	4 + 3 = 7	No	1.1
0.37	4	3 + 4 = 7	No	1.5
0.26	8	4 + 3 = 7	Equivocal	2.9

Table 4 Dominant Pathology Lesion size, Gleason score and PET Detection.

Table 5.

	2D Pelvis		3D Pelvis		WB	
	Average SUV_{max}	Standard Deviation	Average SUV_{max}	Standard Deviation	Average SUV_{max}	Standard Deviation
Prostate Cancer with Positive Uptake (n = 6)	4.7	1.2	3.3	0.6	4.3	1.7
Prostate Cancer with Negative Uptake (n = 7)	1.8	0.6	1.9	0.8	1.7	0.5
Blood Pool (Right Common Femoral Vasculature)	3.8	0.8	2.5	0.4	2.1	0.2
Muscle (Right Gluteus Musculature)	2.0	0.5	1.0	0.2	0.9	0.1

Table 5 Average DCFBC Uptake in Positive and Negative Prostate Cancers as well as Background Blood Pool and Musculature.